Nonlinear dynamics in far-infrared driven quantum-well intersubband transitions

Adriano A. Batista,[1] P. I. Tamborenea,[2] Bjorn Birnir,[3] Mark S. Sherwin,[4] and D. S. Citrin[1]
[1]*School of Electrical and Computer Engineering, Georgia Institute of Technology, Atlanta, Georgia 30332-0250*
[2]*Departamento de Física, FCEN, Universidad de Buenos Aires, C1428EHA Buenos Aires, Argentina*
[3]*Mathematics Department, University of California, Santa Barbara, California 93106*
and Science Institute, University of Iceland, 107 Reykjavik, Iceland
[4]*Department of Physics, University of California, Santa Barbara, California 93106*
(Received 22 April 2002; published 27 November 2002)

We study the effect of many-body interactions on the collective response of confined electrons in doped quantum-well (QW) heterostructures to intense far-infrared radiation. Absorption line shapes are computed both by numerically integrating the equations of motion and by using the appropriately time-averaged equations. For a two-subband double-QW system, optical bistability and period-doubling bifurcations are observed and their parameter range of activity is given. For a three-subband asymmetric triple-QW system driven at $\omega \approx E_2 - E_0$, Hopf bifurcations occur which generate a strong response at a frequency incommensurate with the drive frequency or any natural frequency of the system.

DOI: 10.1103/PhysRevB.66.195325 PACS number(s): 05.45.−a, 78.67.De, 73.21.Fg

I. INTRODUCTION

Hopf bifurcations, with an incommensurate frequency response, and subharmonic generation (a period-doubling bifurcation) are not as ubiquitous features of driven classical nonlinear systems as is superharmonic generation. Although these bifurcations usually require the fine-tuning of parameters, they are being intensively studied due to their numerous applications and theoretical interest.[1,2] The same bifurcations may exist in some driven, effectively nonlinear, quantum mechanical systems. For example, in the mean-field description, Bose-Einstein condensates,[3] Josephson junctions,[4] atomic beams in optical cavities,[5] and *n*-doped quantum wells[6] (QW's) have nonlinear equations of motion. Finding bifurcations in these quantum systems also requires a theoretical or experimental search for the appropriate parameter range. In this article, we focus on strongly driven far-infrared (FIR) intersubband transitions in *n*-doped GaAs/AlGaAs QW's, which have been shown to exhibit superharmonic generation and nonlinear phenomena in their absorption line shapes. We show that the intersubband transitions can undergo Hopf bifurcations and period-doubling bifurcations in their response to a strong FIR drive, and give the appropriate parameter ranges for these effects in chosen QW structures.

In recent years, a number of nonlinear effects have been investigated in *n*-doped QW's. Second-harmonic generation has been accurately simulated and measured.[7–10] The dynamic screening effects on the absorption peak, which depend nonlinearly on the intensity of the incoming radiation, have also been studied experimentally and theoretically. Experiments[7,11] showed the intersubband absorption peak broadening, distorting, and slightly redshifting towards the bare intersubband frequency as the subbands saturate with increasing FIR intensity. These results were in agreement with a two-subband density matrix model proposed by Zalużny.[12,13] Broadening and shifting of the absorption peak occur independent of the QW sheet density and its width. On the other hand, depolarization-shift effects occur only if the QW is wide and many-body interactions are relevant.[14,15] For the same FIR intensity, one sees a few other changes in the absorption such as peak distorting, narrowing, and an additional shift of the peak frequency (which decreases with increasing field intensity).

The electron-electron (e-e) interaction affects the above-mentioned effects in *n*-doped QW's in measurable ways, but it is not a necessary condition for their occurrence. In this article we study a set a nonlinear effects where the main source of the nonlinearities *is* the e-e interaction.

The generic bifurcation from a fixed point (corresponding to a periodic orbit) in a classical system is a Hopf bifurcation (HB),[16] and it typically leads to a response comparable in magnitude to the drive. Another interesting property of this type of response is that it usually happens with a frequency that is incommensurate with the frequency of the drive. These two characteristics motivate the search for a HB from a fixed point in our effectively nonlinear quantum mechanical system. In this paper we show that HB's can be found in suitably designed *n*-doped QW systems driven by intense FIR radiation.

Here we also extend the work of Galdrikian and Birnir[8] and Batista *et al.*[17] on period-doubling bifurcations (PDB's) in a two-subband QW. The theoretical model that we employ here allows the treatment of more than two subbands and in principle can also include exchange-interaction terms and mass dispersion. On the other hand, analytical calculations such as the averaging technique used in Ref. 17 are considerably more difficult to perform when more than two subbands are included in the system. Thus, in those cases we are limited to focusing on numerical results for the nonlinear dynamics.

Many-body effects on intersubband transitions and optical properties of QW's have been studied in recent years[6,18–21] with semiconductor Bloch equations (SBE's) using Hartree-Fock and rotating-wave approximations (RWA's) for the response of two-(sub)band QW's. Multisubband transitions and numerical integration of the SBE's were performed by Tsang *et al.*;[22] however, those authors neglected

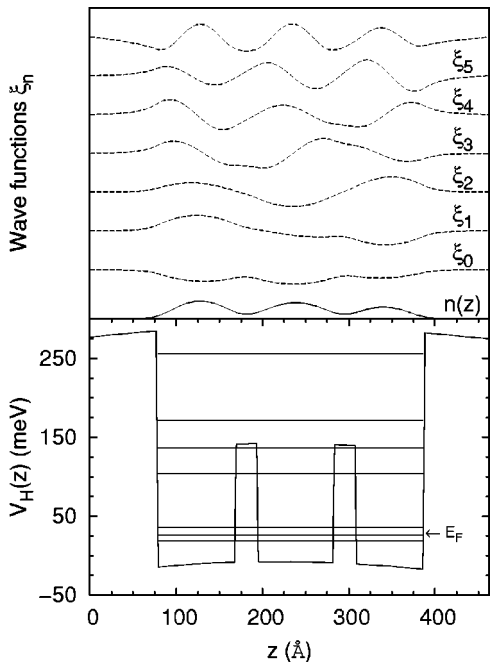

FIG. 1. The stationary self-consistent potential for $N_s=3.0\times10^{11}$ cm^{-2} with the eigenenergies indicated by horizontal bars; the density and first seven eigenstates are shown on top. The double barrier creates, through tunneling, three closely spaced subbands well isolated from upper subbands. The slight asymmetry enhances the nonlinear effects, but too much asymmetry reduces the tunneling and with it the decoupling with upper subbands.

depolarization-shift terms, which is a serious handicap for their predictions for wide QW's.

We study the multisubband SBE's in their time-dependent Hartree version (i.e., without exchange) *without* making the rotating-wave approximation, from a nonlinear dynamical systems perspective. We find, in qualitative agreement with previous work,[8] that for the two-subband QW driven near resonance PDB's or optical bistability (OB) may occur. For a three-subband QW structure (Fig. 1) driven at resonance $\omega=E_{20}$ basically two types of bifurcations occur as the FIR field strength is varied. We observe a HB producing a strong signal at a frequency lower than the frequency of the drive. For a different value of the field strength a PDB is observed that also produces a strong signal. Both of these responses are produced at moderate values of the field strength. In contrast, the PDB signal observed in the double QW in Ref. 8 was much weaker than the fundamental and occurred at relatively large field strength. Our approach can in principle be applied to any multisubband system, with the precaution that the frequencies involved should not exceed the LO phonon energy ($\sim$36 meV in GaAs/AlGaAs QW's), to prevent a rapid loss of coherence.

In Sec. II we start our study of the effect of many-body interactions on the optical properties of confined electrons in δ-doped QW's. We derive the density-matrix equations of motion of the confined electrons, treating the many-body interactions in the time-dependent Hartree approximation. The density matrix provides information on the collective response of the electrons to an applied FIR field. We account for energy (inelastic) and momentum (elastic) types of scattering phenomenologically within the relaxation-time approximation. In Sec. III averaged equations for two-subband QW's and for multisubband QW's are derived; in the latter case the averaging method is applicable only if all the subband energies involved are (almost) equally spaced. In Sec. IV the numerical analysis of the equations obtained in Secs. II and III is shown. Here we confirm previous observations of Galdrikian and Birnir of period-doubling bifurcations for a two-subband system. For a three-subband asymmetric QW with two small barriers we observe Hopf bifurcations of the Poincaré maps in the electrons' collective response.

II. THEORETICAL MODEL

In this section we introduce our theoretical model to describe the interplay of electronic and optical properties of confined electrons in a QW. More specifically, our aim is to understand the influence of the electron-electron interaction on the collective dynamical properties of the electrons when subjected to strong FIR radiation. The starting point is the Hamiltonian of the confined electrons, which includes the interaction of the electrons with the ionized donors located outside the QW's. Our treatment employs the second-quantization formalism, and we use field operators or subband creation and annihilation operators at different stages of the calculations. Initially we do not include the FIR radiation term in the Hamiltonian so that we can understand the origin of the depolarization shift terms and also provide an approximation of the many-body ground state based on the Hartree approximation. This will also give us the basis states for our single-particle field operators, the single-particle energy spectrum, and the equilibrium subband occupation numbers. Afterwards we develop the multisubband time-dependent Hartree theory including the applied FIR field.

A system of fixed donors and confined electrons in a QW with bare potential $W(z)$ has the following Hamiltonian operator:

$$\hat{H}=\hat{H}_0+\hat{H}_{el\text{-}el}+\hat{H}_{el\text{-}b}+H_b\,. \tag{1}$$

The bare well Hamiltonian is given by

$$\hat{H}_0=\int d^3x\,\hat{\psi}^\dagger(x)\left[-\frac{1}{2m^*}\hbar^2\nabla^2+W(z)\right]\hat{\psi}(x).$$

The electron contribution is given by

$$\hat{H}_{el}=\frac{e^2}{2}\int d^3x\int d^3x'\,\hat{\psi}^\dagger(x)\,\hat{\psi}^\dagger(x')\,\frac{1}{|x-x'|}\hat{\psi}(x')\,\hat{\psi}(x).$$

The Hamiltonian for the electron-background interaction is given by

$$\hat{H}_{el-b}=-e^2\int d^3x d^3x'\,\hat{\psi}^\dagger(x')n_D(x)\,\frac{1}{|x-x'|}\hat{\psi}(x'),$$

and the background contribution is

$$H_b=\frac{e^2}{2}\int d^3x\int d^3x'\frac{n_D(x)n_D(x')}{|x-x'|},$$

where $n_D(x)$ denotes the density of the background donors. The field operators $\hat{\psi}(x)$ and $\hat{\psi}^\dagger(x)$ can be expressed as linear combinations of creation and annihilation operators a_k and $a_k^\dagger$, respectively,

$$\hat{\psi}(x)\equiv\sum_k \phi_k(x)a_k,$$

$$\hat{\psi}^\dagger(x)\equiv\sum_k \phi_k^*(x)a_k^\dagger,$$

where the single-particle wave function is $\phi_k(x)=(e^{ik\cdot\rho}/\sqrt{A})\xi_n(z)$ and $\xi_n(z)$ is the envelope wave function in the growth direction. This change of basis will be particularly useful for simplifying the equations of motion from a partial differential equation to an ordinary differential system, in which we will keep only the most important modes.

Using the total Hamiltonian above we obtain the Heisenberg equations of motion for the field operators,

$$i\hbar\frac{\partial\hat{\psi}}{\partial t}(x,t)=\left[-\frac{1}{2m^*}\hbar^2\nabla^2+W(z)\right]\hat{\psi}(x,t)-\int dx' n_D(x')V_\mu(x-x')\hat{\psi}(x,t)+\int dx' V_\mu(x-x')\hat{\psi}^\dagger(x',t)\hat{\psi}(x',t)\hat{\psi}(x,t), \tag{2}$$

where

$$V_\mu(x-x')=\frac{e^2e^{-\mu|x-x'|}}{\kappa|x-x'|}$$

is the screened Coulomb potential, with κ the dielectric constant. The screening is a mathematical artifact included with the only purpose of avoiding divergence in certain integrals; later on we will take the limit $\mu\to 0$ and recover the usual Coulomb potential. In the experimental setup of interest the donors are distributed symmetrically in two thin layers far removed from the QW according to $n_D(z)=N_s/2[\,\delta(z-L)+\delta(z+L)]$, where N_s is the sheet density. The integrals on the right side of Eq. (2) are given by

$$\int dx' n_D(x')V_\mu(x-x')=\frac{\pi e^2N_s}{\kappa\mu}(e^{-\mu|z-L|}+e^{-\mu|z+L|}),$$

$$\int dx' V_\mu(x-x')\hat{\psi}^\dagger(x',t)\hat{\psi}(x',t)=\frac{2\pi e^2}{\kappa A}\sum_{n_1n_2,k_1k_2}a^\dagger_{n_1k_1}a_{n_2k_2}e^{-i\rho\cdot(k_1-k_2)}\int dz'\xi_{n_1}(z')\xi_{n_2}(z')$$
$$\times\int_0^\infty rJ_0(r|k_1-k_2|)\frac{e^{-\mu\sqrt{r^2+(z-z')^2}}}{\sqrt{r^2+(z-z')^2}}dr. \tag{3}$$

The $k_1=k_2$ term in the above sum can be simplified to

$$\frac{2\pi e^2}{\kappa\mu A}\sum_{k,n_1n_2}a^\dagger_{n_1k}a_{n_2k}\int dz'\xi_{n_1}(z')\xi_{n_2}(z')e^{-\mu|z-z'|}=\frac{2\pi e^2}{\kappa\mu A}\left[\hat{N}-\mu\sum_{k,n_1n_2}a^\dagger_{n_1k}a_{n_2k}\int dz'\xi_{n_1}(z')\xi_{n_2}(z')\left|z-z'\right|+O(\mu^2)\right].$$

The diverging terms in Eq. (2) cancel out and we can take the limit $\mu\to 0$, obtaining the depolarization-shift terms in the Heisenberg equation, which becomes

$$i\hbar\frac{\partial\hat{\psi}}{\partial t}(x,t)=\left[-\frac{1}{2m}\hbar^2\nabla^2+W(z)\right]\hat{\psi}(x,t)-\frac{2\pi e^2}{\kappa A}\sum_{k,n_1n_2}a^\dagger_{n_1k}a_{n_2k}\int dz'\xi_{n_1}(z')\xi_{n_2}(z')|z-z'|\hat{\psi}(x,t)$$
$$+\frac{2\pi e^2}{\kappa A}\sum_{n_1n_2,k_1\neq k_2}a^\dagger_{n_1k_1}a_{n_2k_2}e^{-i\rho\cdot(k_1-k_2)}\int dz'\xi_{n_1}(z')\xi_{n_2}(z')\frac{e^{-|k_1-k_2||z-z'|}}{|k_1-k_2|}\hat{\psi}(x,t). \tag{4}$$

After the Hartree approximation is applied, we obtain

$$i\hbar\frac{\partial\hat{\psi}}{\partial t}(x,t)=\left[-\frac{1}{2m^*}\hbar^2\nabla^2+W(z)\right]\hat{\psi}(x,t)-\frac{2\pi e^2}{\kappa A}\sum_{k,n_1}\langle a^\dagger_{n_1k}a_{n_2k}\rangle\int dz'\,\xi_{n_1}(z')\xi_{n_1}(z')|z-z'|\hat{\psi}(x,t). \tag{5}$$

This should be a good approximation for very high sheet densities ($r_s \ll 1$), since the kinetic terms then dominate.[23] There are some studies[24,25] that show a significantly reduced effect of exchange-correlation corrections on the FIR absorption lines in a double QW when two subbands are well populated. The case of the Hartree-Fock approximation will be studied in a following paper.

If $a_n(k,t)=a_n(k)e^{iE_n(k)t}$, where $E_n(k)=E_n+\hbar^2k^2/2m^*$, then $\xi_n(z)$ obeys the Schrödinger equation for the nth-subband wave function given by

$$\left[-\frac{1}{2m^*}\frac{d^2}{dz^2}+W(z)+V_H(z)\right]\xi_n(z)=E_n\xi_n(z). \tag{6}$$

The Hartree potential $V_H(z)$ is given by

$$V_H(z)=\frac{-2\pi e^2}{\kappa}\int_{-\infty}^{\infty}dz'|z-z'|n(z'), \tag{7}$$

and the electron number density is given by

$$n(z)=\langle\hat{\psi}^\dagger(z)\hat{\psi}(z)\rangle=\frac{1}{A}\sum_{n,k}|\xi_n(z)|^2f_n(k), \tag{8}$$

where $f_n(k)$ is the Fermi occupation function. The electron number density can be rewritten as $n(z)=N_s\Sigma_n w_n|\xi_n(z)|^2$, with the normalization $\Sigma_n w_n=1$. The subband occupation numbers at nonzero temperatures are given by

$$w_n=\frac{1}{\pi N_s}\int kdk\,\frac{1}{e^{(E_n(k)-\mu)/T}+1}$$

$$=\frac{m^*T}{\hbar^2N_s\pi}\ln[1+e^{-(E_n-\mu)/T}]. \tag{9}$$

The chemical potential μ can be obtained from solving the polynomial equation

$$N_s=\frac{m^*T}{\pi\hbar^2}\sum_n\ln[1+e^{-(E_n-\mu)/T}], \tag{10}$$

where the variable is $e^{-\mu/T}$. It can be easily proved that there is only one solution for μ real. For the two-subband case we can actually solve this equation analytically. We obtain

$$w_0=\frac{m^*T}{\hbar^2N_s\pi}\ln\{1+e^{\delta/T}[-\cosh(\delta/T)+\sqrt{\sinh^2(\delta/T)+s}]\},$$

$$w_1=\frac{m^*T}{\hbar^2N_s\pi}\ln\{1+e^{-\delta/T}[-\cosh(\delta/T)+\sqrt{\sinh^2(\delta/T)+s}]\},$$

where $\delta=(E_1-E_0)/2$ and $s=\exp[\pi\hbar^2N_s/m^*T]$. At $T=0$ the subband occupation numbers are given by

$$w_n=\frac{m^*}{\pi\hbar^2N_s}(\mu-E_n)\Theta(\mu-E_n) \tag{11}$$

and the chemical potential can be obtained from self-consistently solving

$$N_s=\frac{m^*}{\pi\hbar^2}\sum_n(\mu-E_n)\Theta(\mu-E_n), \tag{12}$$

where Θ is the step function.

Now using the electric-dipole approximation we include the external FIR field, polarized in the growth direction, in the Heisenberg equations [in Eq. (4)]. This introduces coherence between states of different subbands but with the same momentum. Neglecting the coherence between states with different momentum is a valid approximation since the momentum transfer due to the THz radiation is negligible due to the small energy differences between subbands (of the order of 10 meV). With this external field, the Heisenberg equation in the time-dependent Hartree approximation becomes

$$i\hbar\frac{\partial\hat{\psi}}{\partial t}(x,t)=\left[-\frac{1}{2m^*}\hbar^2\nabla^2+W(z)+V_H(z)\right]\hat{\psi}(x,t)$$

$$-\frac{2\pi e^2}{\kappa A}\sum_{k,n_1n_2}[\langle a^\dagger_{n_1k}a_{n_2k}\rangle-f_{n_1}(k)\delta_{n_1,n_2}]$$

$$\times\int dz'\,\xi_{n_1}(z')\xi_{n_2}(z')|z-z'|\hat{\psi}(x,t)$$

$$-eF(t)z\hat{\psi}(x,t). \tag{13}$$

After rewriting the above equation solely in terms of the operators a_{nk} and $a^\dagger_{n'k}$, we obtain

$$i\hbar\dot{a}_{n'p}=E_n(p)a_{n'p}-\frac{2\pi e^2}{\kappa A}\sum_{k,n_1n_2n_3}[\langle a^\dagger_{n_1k}a_{n_2k}\rangle$$

$$-f_{n_1}(k)\delta_{n_1,n_2}]\int dz\int dz'\,\xi_{n'}(z)\xi_{n_1}(z')$$

$$\times|z-z'|\xi_{n_2}(z')\xi_{n_3}(z)a_{n_3p}-\sum_m F(t)\mu_{n'm}a_{pm}.$$

The density matrix provides information on the far-infrared response to the THz field of the electrons collective oscillations in the QW. It also allows us to treat dissipation effects due to momentum scattering with point impurities and energy scattering with phonons. The elements of the density matrix are given by

$$\sigma_{nn'}(k)=\langle a^\dagger_{nk}a_{n'k}\rangle. \tag{14}$$

With this substitution and the shorthand notation

$$V^0_{n_1n_2n_3n_4}=\frac{2\pi e^2N_s}{\kappa}\int dz\int dz'\,\xi_{n_1}(z)\xi_{n_2}(z')\times|z-z'|\xi_{n_3}(z')\xi_{n_4}(z), \tag{15}$$

we obtain

$$i\hbar\dot{a}_{n'p}=E_{n'}(p)a_{n'p}-\frac{1}{AN_s}\sum_{k,n_1n_3n_4}V^0_{n'n_2n_3n_4}[\sigma_{n_2n_3}(k)-f_{n_2}(k)\delta_{n_2,n_3}]a_{n_4p}-\sum_m F(t)\mu_{n'm}a_{mp}.$$

Multiplying the above equation to the left by $a^\dagger_{pn}$ and then applying the quantum statistical average, denoted by the angular brackets, we obtain

$$\begin{aligned}-i\hbar\langle a^\dagger_{np}\dot{a}_{n'p}\rangle=&-E_{n'}(p)\sigma_{nn'}(p)\\&+\frac{1}{AN_s}\sum_{k,n_2n_3n_4}V^0_{n'n_2n_3n_4}[\sigma_{n_2n_3}(k)\\&-f_{n_2}(k)\delta_{n_2n_3}]\sigma_{nn_4}(p)\\&+\sum_m F(t)\mu_{n'm}\sigma_{nm}(p).\end{aligned}$$

Another approximation we introduce is to consider the effective masses of all subbands equal, which is a fairly accurate approximation for GaAs/AlGaAs QW's. (This is not the case in general; for example, it does not apply to InAs/AlSb QW's.) With this approximation, we can reduce the dimensions of the equation of motion even further by performing a sum over k. Then the equations for the averaged density matrix become

$$\begin{aligned}-i\hbar\dot{\sigma}_{nn'}=&(E_n-E_{n'})\sigma_{nn'}+i\Gamma_{nn'}(\sigma_{nn'}-\sigma^0_{nn'})\\&+\sum_{n_2n_3n_4}V^0_{n'n_2n_3n_4}\sigma_{nn_4}(\sigma_{n_2n_3}-\sigma^0_{n_2n_3})\\&-\sum_{n_1n_2n_3}V^0_{n_1n_2n_3n}\sigma_{n_1n'}(\sigma_{n_2n_3}-\sigma^0_{n_2n_3})\\&-\sum_m F(t)(\mu_{mn}\sigma_{mn'}-\mu_{n'm}\sigma_{nm}),\end{aligned} \tag{16}$$

where $\sigma_{nn'}=(1/AN_s)\Sigma_k\sigma_{nn'}(k)$ and $\sigma^0_{nn'}$ is the equilibrium density matrix. We introduced above, within the relaxation-time approximation, the phenomenological dissipation rates $\Gamma_{nn'}=\hbar\delta_{nn'}/T_1+\hbar(1-\delta_{nn'})/T_2$, where T_1 is the energy scattering time (or depopulation time) and T_2 is the momentum scattering time (or depolarization time). Before proceeding further, it is useful to transform the above equations into dimensionless form via

$$\tau=\Omega t,\quad \epsilon_{nn'}=\frac{E_n-E_{n'}}{\hbar\Omega},\quad \gamma_{nn'}=\frac{\Gamma_{nn'}}{\hbar\Omega},\quad \tilde{\mu}_{mn}=\frac{\mu_{mn}}{\mu_{10}},$$

$$\mathcal{E}(t)=\frac{\mu_{10}F(t)}{\hbar\Omega},\quad \mathcal{V}^0_{n_1n_2n_3n_4}=\frac{1}{\hbar\Omega}V^0_{n_1n_2n_3n_4}, \tag{17}$$

where Ω is the frequency of the driving field. After these transformations one obtains

$$\begin{aligned}-i\dot{\sigma}_{nn'}=&\epsilon_{nn'}\sigma_{nn'}+i\gamma_{nn'}(\sigma_{nn'}-\sigma^0_{nn'})\\&+\sum_{n_2n_3n_4}\mathcal{V}^0_{n'n_2n_3n_4}\sigma_{n,n_4}(\sigma_{n_2n_3}-\sigma^0_{n_2n_3})\\&-\sum_{n_1n_2n_3}\mathcal{V}^0_{n_1n_2n_3n}\sigma_{n_1n'}(\sigma_{n_2n_3}-\sigma^0_{n_2n_3})\\&-\sum_m(\tilde{\mu}_{mn}\sigma_{mn'}-\tilde{\mu}_{n'm}\sigma_{nm})\mathcal{E}(\tau).\end{aligned} \tag{18}$$

The main advantage of the present method based on field operators over the method used in Ref. 8 is that now we have developed the density-matrix equations of motion for any number of subbands. The previous method is restricted to the two-subband problem without exchange terms. The exchange terms could also be included in our equations once the time-dependent Hartree-Fock approximation is taken.

Two-subband problem

In the two-subband system case Eqs. (18) can be explicitly written as

$$\begin{aligned}\dot{\sigma}_{00}=&-\gamma_1(\sigma_{00}-\sigma^0_{00})-i\sum_{n_2n_3}\mathcal{V}^0_{0n_2n_31}(\sigma_{n_2n_3}-\sigma^0_{n_2n_3})\\&\times(\sigma_{10}-\sigma_{01})-i\mathcal{E}(\tau)(\sigma_{10}-\sigma_{01}).\end{aligned} \tag{19}$$

With the substitution of

$$\begin{aligned}\sum_{n_2n_3}\mathcal{V}^0_{0n_2n_31}(\sigma_{n_2n_3}-\sigma^0_{n_2n_3})=&2\mathcal{V}^0_{0101}\mathrm{Re}\sigma_{10}\\&+\mathcal{V}^0_{0001}(\sigma_{00}-\sigma^0_{00})\\&+\mathcal{V}^0_{0111}(\sigma_{11}-\sigma^0_{11})\end{aligned} \tag{20}$$

and $\sigma_{00}=(1+\Delta)/2$ in the above equation, we obtain

$$\begin{aligned}\dot{\Delta}=&-\gamma_1(\Delta-\Delta_0)+8\mathrm{Im}\sigma_{10}[\mathcal{V}^0_{0101}\mathrm{Re}\sigma_{10}\\&+(\mathcal{V}^0_{0001}-\mathcal{V}^0_{0111})(\Delta-\Delta_0)/4+\mathcal{E}(t)/2].\end{aligned}$$

The equation for the coherence term is given by

$$\begin{aligned}\dot{\sigma}_{10}=&i\epsilon_{10}\sigma_{10}-\gamma_2\sigma_{10}-i\Delta\sum_{n_2n_3}\mathcal{V}^0_{0n_2n_31}(\sigma_{n_2n_3}-\sigma^0_{n_2n_3})\\&-i\sigma_{10}\sum_{n_2n_3}(\mathcal{V}^0_{1n_2n_31}-\mathcal{V}^0_{0n_2n_30})(\sigma_{n_2n_3}-\sigma^0_{n_2n_3})\\&-i\mathcal{E}(\tau)\sum_m(\tilde{\mu}_{m1}\sigma_{m0}-\tilde{\mu}_{0m}\sigma_{1m}).\end{aligned}$$

Making the simplifications

$$\sum_{n_2 n_3} \mathcal{V}^0_{0 n_2 n_3 1}(\sigma_{n_2 n_3}-\sigma^0_{n_2 n_3}) = 2\mathcal{V}^0_{0101}\mathrm{Re}\sigma_{10} + (\mathcal{V}^0_{0001}-\mathcal{V}^0_{0111}) \times(\Delta-\Delta_0)/2,$$

$$\sum_{n_2 n_3} (\mathcal{V}^0_{1 n_2 n_3 1}-\mathcal{V}^0_{0 n_2 n_3 0})(\sigma_{n_2 n_3}-\sigma^0_{n_2 n_3}) = 2(\mathcal{V}^0_{0111}-\mathcal{V}^0_{0001})\mathrm{Re}\sigma_{10} + (2\mathcal{V}^0_{1001}-\mathcal{V}^0_{0000}-\mathcal{V}^0_{1111}) \times(\Delta-\Delta_0)/2,$$

$$\sum_m (\tilde{\mu}_{m1}\sigma_{m0}-\tilde{\mu}_{0m}\sigma_{1m}) = \Delta + (\tilde{\mu}_{11}-\tilde{\mu}_{00})\sigma_{10},$$

we obtain

$$\begin{aligned}
\dot{\Delta} &= -\gamma_1(\Delta-\Delta_0) + 4\mathrm{Im}\sigma_{10} \times\{\alpha[\mathrm{Re}\sigma_{10}-\zeta(\Delta-\Delta_0)/4]+\mathcal{E}(\tau)\},\\
\dot{\sigma}_{10} &= i\tilde{\epsilon}_{10}\sigma_{10}-\gamma_2\sigma_{10}-i\alpha\Delta[\mathrm{Re}\sigma_{10}-\zeta(\Delta-\Delta_0)/4] - i\alpha\sigma_{10}[\zeta\mathrm{Re}\sigma_{10}+\beta(\Delta-\Delta_0)/4] - i\mathcal{E}(\tau)[\mu_{10}\Delta+(\mu_{11}-\mu_{00})\sigma_{10}],
\end{aligned} \tag{21}$$

where we have used the shorthand notation $\alpha = 2V^0_{0101}$, $\zeta = (V^0_{1101}-V^0_{1000})/V^0_{1010}$, and $\beta = (2V^0_{1001}-V^0_{0000}-V^0_{1111})/V^0_{1010}$. We can further simplify Eq. (21) with the notation $V_{10}(\tau) = \mathcal{E}(\tau)+\alpha[\mathrm{Re}\sigma_{10}-\zeta(\Delta-\Delta_0)/4]$, which results in

$$\begin{aligned}
\dot{\Delta} &= -\gamma_1(\Delta-\Delta_0) + 4\mathrm{Im}\sigma_{10}V_{10}(\tau),\\
\dot{\sigma}_{10} &= i\tilde{\epsilon}_{10}\sigma_{10}-\gamma_2\sigma_{10}-i\Delta V_{10}(\tau) - i\sigma_{10}\{\alpha[\zeta\mathrm{Re}\sigma_{10}+\beta(\Delta-\Delta_0)/4]+\mathcal{E}(\tau)(\tilde{\mu}_{11}-\tilde{\mu}_{00})\}.
\end{aligned} \tag{22}$$

This equation is equivalent to the one found previously by Galdrikian and Birnir.[8] In the next section we approximate the original system (18) by a simplified set of equations which allows us to do some predictions of OB's. The validity of the method is verified by comparing its predictions with some of our numerical results.

III. AVERAGING METHOD

The averaging method is generally used to eliminate the explicit time dependence of periodically driven ODE systems. It has been applied in many different problems, e.g., the gravitational three-body problem, the van der Pol oscillator,[2] and in the study of PDB's in the Duffing oscillator.[1] The simplest application of this method is perhaps the computation of the shape of the first two Arnold tongues (i.e., the boundary between stable and unstable motion) in Mathieu's equation.[26] A survey of the theory of averaging and many new results can be found in Ref. 27. Next we present a brief summary of this method.

Suppose we have a differential equation

$$\dot{x} = \epsilon f(x,t), \quad x\in\mathbf{C}^n, \quad 0<\epsilon\ll 1, \tag{23}$$

with $f(x,t)$ T periodic and sufficiently well behaved (C^2 is enough). The function f can be decomposed in its Fourier modes, $f(x) = f_0(x)+\tilde{f}(x,t)$, where $f_0(x)$ has no explicit time dependence and $\tilde{f}(x,t)$ includes all the oscillating terms. The averaging theorem[2,1] states that in the limit $\epsilon\to 0$, Eq. (23), through the transformation $x = y+\epsilon w(y,t)$, can be replaced by

$$\dot{y} = \epsilon f_0(y) + \epsilon^2 D\tilde{f}(y,t)w(y,t).$$

The function $w(y,t)$ is chosen to satisfy the differential equation $w_t(y,t) = \tilde{f}(y,t)$ with integration constants set to zero. Since here we are interested only in first-order averaging, we neglect terms $O(\epsilon^2)$. We are then left with

$$\dot{y} = \epsilon f_0(y). \tag{24}$$

This replacement means that for the same initial conditions solutions to Eqs. (23) and (24) will be close to order $O(\epsilon)$ in a time scale of $O(1/\epsilon)$. Therefore a study of Eq. (24) reveals substantial information about the structure of the original system (23).

The averaging method will be applied to the multisubband case in which the energy levels are (almost) equally spaced or only have small deviations from it. This condition can be relaxed but the equations become slightly more complicated to write; however, the algorithm to solve them has the same complexity. Applying the transformation $\sigma_{nn'}-\sigma^0_{nn'} = \exp[i(n-n')\omega t]\rho_{nn'}$ to Eqs. (16) we can set them into the slowly varying form if we assume that the dissipation rates, Coulomb interaction coefficients, and $\mu_{nm}F(t)$ are small compared to $\hbar\Omega$. The resulting equations are

$$\begin{aligned}
-i\hbar\frac{\partial}{\partial t}\rho_{nn'} &= (\mathcal{D}_{nn'}+i\Gamma_{nn'})\rho_{nn'} + e^{-i(n-n')\omega t}\sum_{n_2 n_3 n_4} V^0_{n' n_2 n_3 n_4}(\rho_{n,n_4}e^{i(n-n_4)\omega t}+\sigma^0_{n n_4})\rho_{n_2 n_3}e^{i(n_2-n_3)\omega t}\\
&- e^{-i(n-n')\omega t}\sum_{n_2 n_3 n_4} V^0_{n n_2 n_3 n_4}(\rho_{n_4,n'}e^{i(n_4-n')\omega t}+\sigma^0_{n_4 n'})\rho_{n_2 n_3}e^{i(n_2-n_3)\omega t} - e^{-i(n-n')\omega t}\sum_m (\mu_{mn}\rho_{mn'}e^{i(m-n')\omega t}\\
&- \mu_{n'm}\rho_{nm}e^{i(n-m)\omega t})F(t) - e^{-i(n-n')\omega t}\mu_{n'n}(\sigma^0_{n'n'}-\sigma^0_{nn})F(t).
\end{aligned} \tag{25}$$

The applied external field is given by $F(t)=F_0e^{i\Omega t}+F_0^*e^{-i\Omega t}$, where $\Omega=N\omega$ with N integer, $\mathcal{D}_{nn'}=E_n-E_{n'}-\hbar(n-n')\omega$, and the field strength F_0 is a constant. After transforming the above equations to dimensionless form via Eq. (17) we can see that the right-hand side of the above equation has an explicit time dependence which is periodic with frequency ω/Ω and is weakly varying in time. Thus the averaging method can be correctly applied and to first order we obtain

$$-i\frac{\partial}{\partial\tau}\rho_{nn'}=(\tilde{\mathcal{D}}_{nn'}+i\gamma_{nn'})\rho_{nn'}+\sum_{n_2n_3n_4}\mathcal{V}^0_{n'n_2n_3n_4}(\rho_{n,n_4}\delta_{n'+n_2,n_3+n_4}+\sigma^0_{nn_4}\delta_{n'+n_2,n_3+n})\rho_{n_2n_3}$$
$$-\sum_{n_2n_3n_4}\mathcal{V}^0_{nn_2n_3n_4}(\rho_{n_4,n'}\delta_{n_2+n_4,n+n_3}+\sigma^0_{n_4n'}\delta_{n'+n_2,n+n_3})\rho_{n_2n_3}-\sum_m[\tilde{\mu}_{mn}\rho_{mn'}(\mathcal{E}_0\delta_{m-n,-N}+\mathcal{E}_0^*\delta_{m-n,N})$$
$$-\tilde{\mu}_{n'm}\rho_{nm}(\mathcal{E}_0\delta_{n'-m,-N}+\mathcal{E}_0^*\delta_{n'-m,N})]-(\mathcal{E}_0\delta_{n-n',N}+\mathcal{E}_0^*\delta_{n-n',-N})\tilde{\mu}_{n'n}(\sigma^0_{n'n'}-\sigma^0_{nn}). \quad (26)$$

Now we can integrate these equations numerically until they converge to a fixed point which gives the response of the system. First-order averaging will give us an equivalent answer to that of the RWA when the latter is applicable, but the range of applicability of the averaging method is larger than the RWA's. For instance, the RWA does not apply for a multiple-subband problem when the intersubband spacing is nearly constant as just described. There are other handicaps of the RWA even for a two-subband system. For example, the RWA cannot account for second-harmonic generation in asymmetric QW's when the drive frequency $\Omega\approx\epsilon_{10}/2$ and it cannot describe subharmonic generation either.[17] For these last two problems one needs to go to second order in the averaging method.

A. Optical bistability in the two-subband QW

Optical bistability is basically a nonlinear response of the medium (here confined electrons in a QW) to an external oscillating field, in which there are three possible responses (two stable and one unstable). Which one the system chooses depends on the history of the adiabatically varying control parameters (usually electric field amplitude). *The OB we consider here is an intrinsic feature of the electron gas in the QW and does not rely on the use of a Fabry-Perot resonator*. In addition, the effect is due to coupling of the far-infrared radiation to intersubband transitions in the QW. Another feature of OB is that it is not a ubiquitous nonlinear response such as superharmonic generation; it can be observed only at some restricted values of the parameters. Furthermore, the nonlinear response changes abruptly from one value of the output to the other at a saddle-node bifurcation when the unstable fixed point merges with the stable fixed point the system was at. This effect can be measured by detecting the different transmitted intensities of the FIR field to the same input field. The two stable responses have different phases; the low-transmissivity one corresponds to in-phase oscillations with the external field (the electron population is higher in the lower well) while the high-transmissivity solution corresponds to out-of-phase oscillations with the external field (the electron population is higher in the upper well). These transmission features of OB make it a relevant choice for applications to optical switching and the realization of optical logic gates.[28]

The innovation of our approach over the previous studies in Ref. 28 lies in the absence of cavities (etalons), the inexistence of any external dc bias, in the fact that the frequency range of the drive is in the THz, and in the essential role played by the many-body interactions. Intrinsic OB was studied in Ref. 29 in a similar setting to ours, but in their model they neglected depolarization shift and coherence effects (since they used only a rate-equation model); these two ingredients though are essential for the OB observed here. Two other studies[13,30] proposed density-matrix models describing the intrinsic OB of *n*-doped QW's, but they were both limited to the RWA and they did not verify the applicability range of their results. Although in Ref. 30 a four-subband basis is used, while in our present study of OB we have a two-subband basis, their analysis of the equations of motion is purely numerical and a parameter range of OB activity is not provided.

Let us apply the averaging method to first order to Eqs. (23). We will calculate the absorption line and compare it with the results we obtain from solving numerically the density matrix equations for a two-subband QW. After making the transformation $\sigma_{10}=\sigma e^{i\tau}$ we perform first-order averaging (the same as the RWA) to Eqs. (23). We obtain the following equations for both symmetric and asymmetric QW's:

$$\dot{\Delta}=-\gamma_1(\Delta-\Delta_0)-i\mathcal{E}_0(\sigma-\sigma^*),$$
$$\dot{\sigma}=(i\delta-\gamma_2)\sigma-i\frac{\alpha\Delta}{2}\sigma-i\alpha\sigma\beta(\Delta-\Delta_0)/4-i\mathcal{E}_0\Delta/2, \quad (27)$$

where $\delta=\epsilon_{10}-1$ is the detuning. The next step is to find the true fixed point of Eq. (28), which is given by

$$\sigma=\frac{i\mathcal{E}_0\Delta/2}{-\gamma_2+i[\delta-\alpha\Delta/2-\alpha\beta(\Delta-\Delta_0)/4]}, \quad (28)$$

whose imaginary part is

$$\mathrm{Im}\sigma=\frac{-\mathcal{E}_0\Delta\gamma_2/2}{[\delta-\alpha(1+\beta/2)(\Delta-\Delta_0)/2]^2+\gamma_2^2}, \quad (29)$$

where $\bar{\delta}=\delta-\alpha\Delta_0/2$. Then we substitute this expression in the equation for Δ obtaining a cubic equation in the population difference:

$$\gamma_1(\Delta-\Delta_0)+\frac{\mathcal{E}_0^2\Delta\gamma_2}{[\bar{\delta}-\alpha(1+\beta/2)(\Delta-\Delta_0)/2]^2+\gamma_2^2}=0. \tag{30}$$

We can simplify the above equation using the shorthand notation $y=\alpha(1+\beta/2)(\Delta-\Delta_0)/2$. With this substitution we obtain the cubic in y:

$$[(\bar{\delta}-y)^2+\gamma_2^2]y+\frac{\mathcal{E}_0^2\gamma_2}{\gamma_1}y+\frac{\alpha\Delta_0\mathcal{E}_0^2\gamma_2}{2\gamma_1}\left(1+\frac{\beta}{2}\right)=0. \tag{31}$$

In principle we can solve a generic cubic equation exactly; however, it is not really illuminating to do this, but it is useful to know under which conditions it is possible to have three real solutions. This region characterizes an optical bistability. A necessary condition for its existence is given by

$$D=-\bar{\delta}^2/3+\gamma_2^2+\mathcal{E}_0^2\frac{\gamma_2}{\gamma_1}<0, \tag{32}$$

and a sufficient condition is

$$-2\left(\frac{-D}{3}\right)^{3/2}<C<2\left(\frac{-D}{3}\right)^{3/2}, \tag{33}$$

where

$$C=\frac{2\bar{\delta}^3}{27}+\frac{2}{3}\left(\gamma_2^2+\mathcal{E}_0^2\frac{\gamma_2}{\gamma_1}\right)\bar{\delta}+\frac{\alpha\Delta_0\mathcal{E}_0^2\gamma_2}{2\gamma_1}\left(1+\frac{\beta}{2}\right).$$

B. Absorption

We would like to know what the effect of many-body interactions of confined electrons in a *n*-doped QW on its absorption line shapes is. We obtain our results by both integrating numerically the full equations of motion and using the averaged ones. The amount of work the driving field makes per period of the drive and per electron is given by

$$G=\frac{1}{NT}\sum_i\int_0^T dt\, eE_i(t)\frac{d}{dt}\langle z_i(t)\rangle, \tag{34}$$

where the sum is over all electrons in the QW. We assume here that all electrons have the same velocity; i.e., they are oscillating in a long-wavelength plasmon mode. We obtain

$$G=\frac{1}{T}\int_0^T dt\, eE(t)\frac{d}{dt}\mathrm{Tr}[\sigma(t)z], \tag{35}$$

which for a two-subband system reduces to

$$G=\frac{1}{T}\int_0^T dt\, eE(t)z_{10}[-\zeta\dot{\Delta}+2\mathrm{Re}\dot{\sigma}_{10}(t)]. \tag{36}$$

We can substitute the result obtained from Eq. (22) and obtain an expression that depends only on the density matrix.

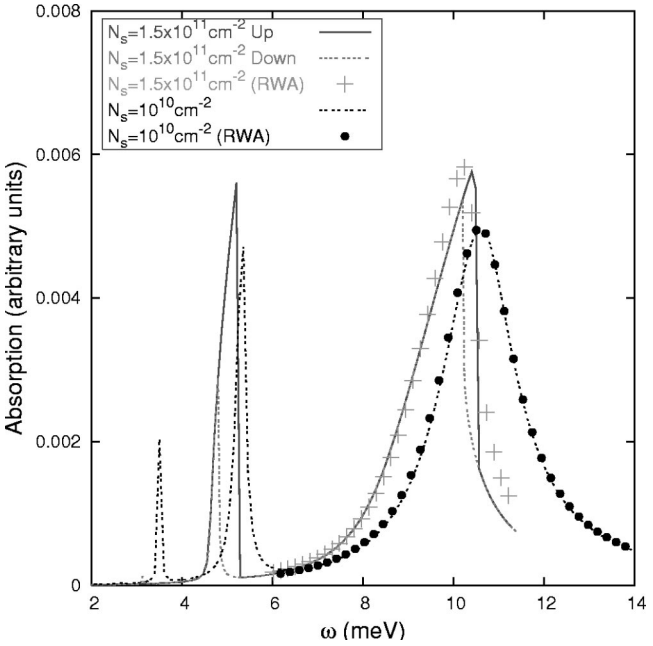

FIG. 2. Comparison of numerical absorption lines with absorption lines calculated with the RWA for a two-subband asymmetric double well with sheet densities given in the figure. The bare QW intersubband gap is 10.6 meV. The optical bistability occurs at sheet density $N_s=1.5\times10^{11}$ cm^{-2} near $\omega=10.5$ meV. The FIR field amplitude is about 1.4 kV/cm, which significantly enhances the line broadening of the absorption curves.

For the many-subband case in general we have to resort to the numerical results given by Eq. (35), except when the subband energies are almost equally spaced. In this situation we can use Eq. (26) and obtain

$$G=-2e\omega\sum_{n>m}(n-m)(\mathcal{E}_0\delta_{n-m,-N}+\mathcal{E}_0^*\delta_{n-m,N})\tilde{\mu}_{mn}\mathrm{Im}\rho_{nm}. \tag{37}$$

IV. NUMERICAL RESULTS

The double-QW structures used are 310 Å wide and 200 meV deep with one barrier of 50 Å in width and 50 meV in height; in the asymmetric double QW this barrier is 25 Å off the center. The triple-QW structure studied is 310 Å wide and 300 meV deep with two barriers of 26 Å in width and 150 meV in height. The leftmost barrier is located at 92 Å from the left edge of the QW and the distance between the two barriers is 88 Å. Figure 1 shows the effective well shape with a sheet density $N_s=3.0\times10^{11}$ cm^{-2} (provided by Si-δ-doped donor layers set back at hundreds of angstroms from both sides of the QW). Equation (18) for the case of two and three subbands was integrated using the fourth-order Runge-Kutta method with 2048 steps per cycle of drive. After an equilibration time of 1000 cycles of the FIR field, the data (plotted in Figs. 2–11) was taken over 128 cycles. These results are obtained at the temperature $T=0$, but we verified in triple QW's that they are approximately the same for T up to 50 K; the nonlinearity is substantially reduced for T

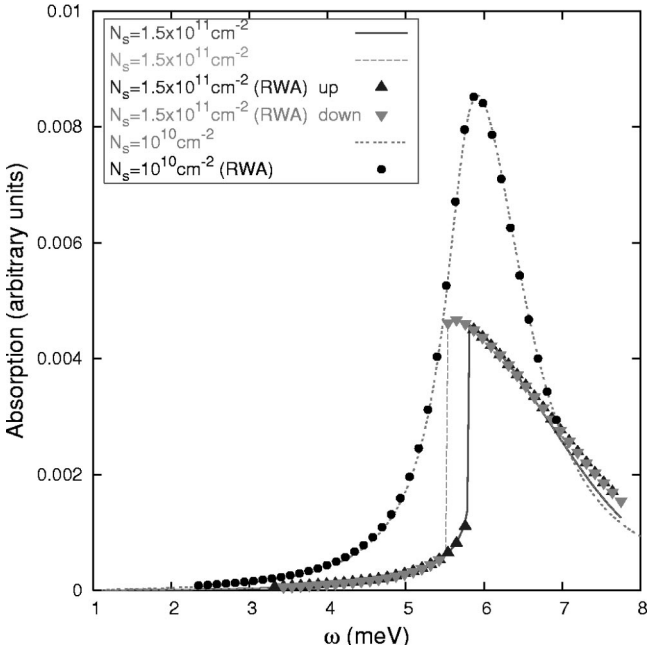

FIG. 3. Comparison of numerical absorption lines with absorption lines calculated with the RWA for a two-subband symmetric double QW with sheet densities given in the figure. The bare QW intersubband gap is 5.9 meV. The optical bistability occurs at sheet density $N_s = 1.5 \times 10^{11}\ \mathrm{cm}^{-2}$ with FIR frequency range $\omega = 5.4$–5.9 meV. The data with up-pointed triangles was taken with adiabatically increasing ω, while the down-pointed ones where taken with decreasing ω. The FIR field amplitude is about 0.7 kV/cm.

>100 K. For the OB and PDB results in the double QW the relaxation times used were $T_1 = T_2 = 6.58$ ps ($\Gamma_1 = \Gamma_2 = 0.1$ meV) and for the HB's results in the triple QW we used $T_1 = T_2 = 65.8$ ps ($\Gamma_1 = \Gamma_2 = 0.01$ meV). We also verified that the HB's still occur for a depolarization time T_2 as low as 6.58 ps while T_1 was kept at 65.8 ps. T_1 is roughly the experimentally measured depopulation time for a two-

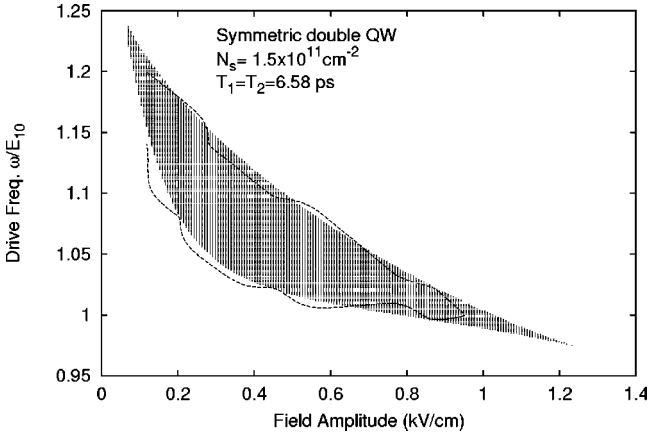

FIG. 4. Range of optical bistability activity of the long-wavelength intersubband plasmons of the confined electrons in the double QW driven by a FIR field. The shaded area was obtained in the RWA in Eq. (28) while the dashed contour line was obtained from the numerical integration of Eq. (23).

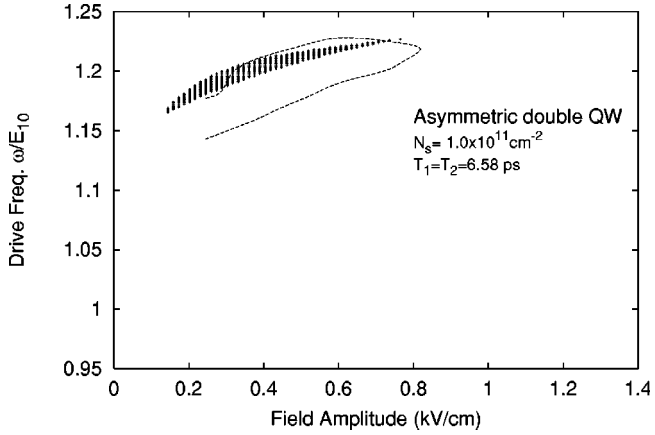

FIG. 5. Range of optical bistability activity in the asymmetric double QW. The shaded area was obtained from Eq. (28) while the contour line was obtained from the numerical integration of Eq. (23).

subband QW,[9,31] but T_2 for the results displayed here is about one order of magnitude higher than what was found more recently in Refs. 32 and 33. Although they found larger values of T_2 than in Refs. 9 and 31 and point out that the most important contributions for the intersubband plasmon absorption linewidth[34] come from interface roughness of the QW walls and point impurities. One can expect then that as QW growth techniques improve these sources of scatterings will be decreased and our values of T_2 could be achievable. The FIR field driving the triple QW in Figs. 7–10 has frequency $\omega = E_{20}$, which is ≈ 5 THz (or 20 meV) and is well in the range of the free-electron laser (however, E_{20} can be lowered by decreasing the tunneling if necessary).

A. Absorption and optical bistability

Figures 2 and 3 (for double QW's) and Fig. 6 (for the three-subband QW) show a very good agreement in the com-

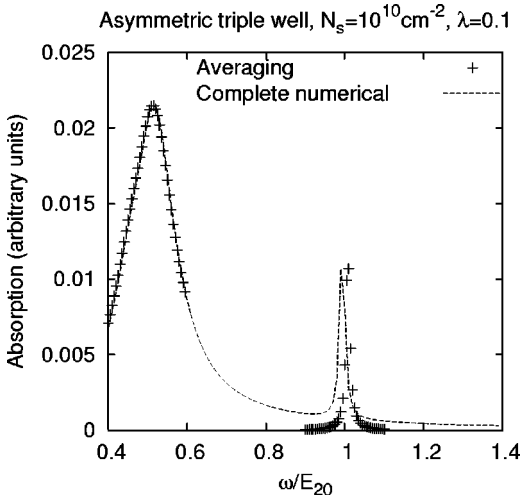

FIG. 6. Comparison of numerical absorption lines with absorption lines calculated with the averaged equations (26) and (37) for a three-subband asymmetric triple well with sheet density given in the figure. Note that the large broadening of the first resonance peak is due to the relatively high field intensity.

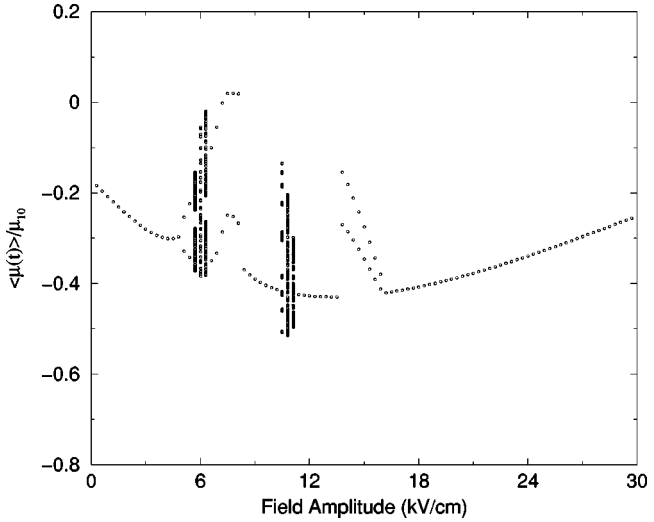

FIG. 7. The Poincaré map of the scaled dipole moment in the doped QW with $N_s=3.0\times10^{11}$ cm^{-2}. The time evolution of the dipole moment is provided by the density matrix with $\langle\mu(t)\rangle = \mathrm{tr}\{\mu\,\sigma(t)\}$. As the field strength increases a PDB occurs at 5.1 kV/cm. The two branches of the PDB undergo a HB at 5.7 kV/cm. At 11.34 kV/cm a supercritical HB occurs, as the field is decreased below this value.

puted absorption lines obtained from the original equations (28) and those obtained from the averaged equation (22). These results are in qualitative agreement with the observed line broadening and distorting of the resonance peak due to high-intensity fields in a double QW in experiments by Craig *et al.*[11]; they are also similar to Zalużny's results[13] for the optical bistability in two-subband asymmetric QW's. In Fig. 4 we show the zone of OB activity in a symmetric double QW as predicted by the RWA of the density-matrix equations and by its full numerical integration. In Fig. 5 we show equivalent results for an asymmetric QW but with less agreement between RWA results and fully numerical results. This should remind us that for the same parameters except for the

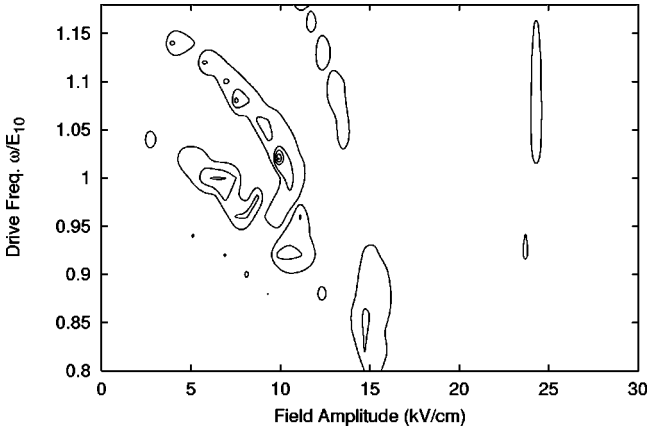

FIG. 8. A contour plot of the zones of nonlinear response with either HB or PDB response. The level sets in the figure give the difference between maximum and minimum dipole moments obtained at each value of field amplitude and frequency from Poincaré maps such as the one in Fig. 7.

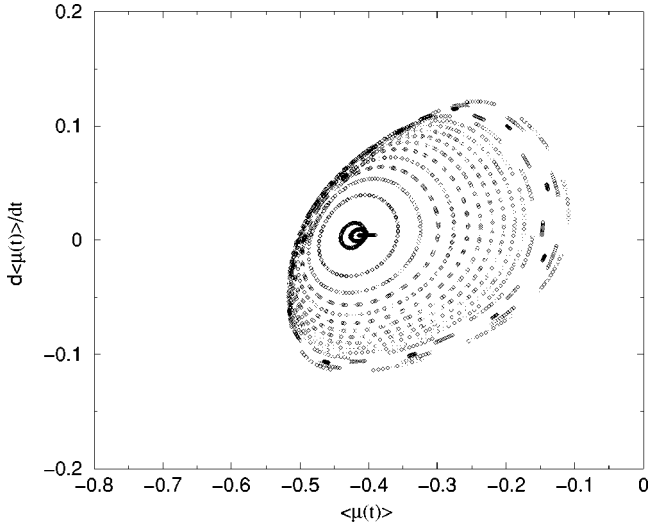

FIG. 9. Phase portrait view of the Hopf bifurcation in the QW. Each one of the closed orbits corresponds to a different value of the field amplitude in the range 10.2–11.4 kV/cm.

QW shape the RWA may not always work. As seen in the figures it works better for symmetric QW's. These results could serve as a useful guide for the experimentalist in search of an OB response in QW's.

In Fig. 6 we show that the averaging method works well, predicting the absorption line of a three-subband QW. In principle we can go further, making a more thorough analysis of absorption lines of multiple-subband QW's, but that will be left for a future work. For now we just wanted to point out that the averaging method can be a very good technique in studying multilevel systems in which the RWA does not always work.

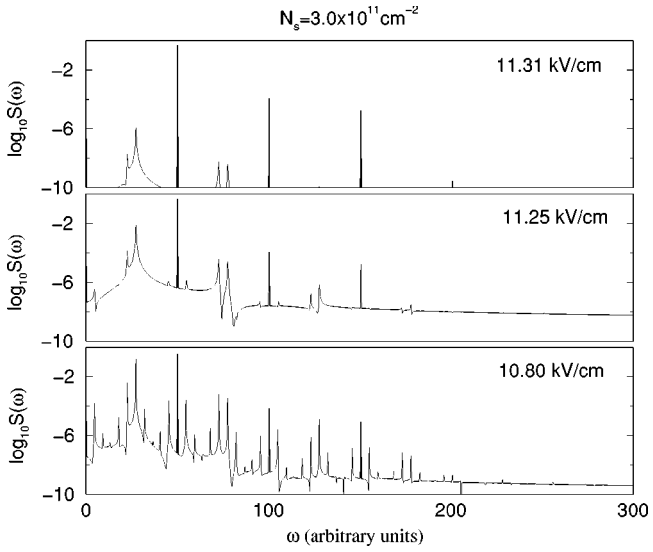

FIG. 10. Power spectra of the dipole moment for the doped asymmetric QW near the onset of the supercritical Hopf bifurcation. As we decrease the field past 11.34 kV/cm the low-frequency signal grows continuously. The zero-frequency peak coincides with the *y* axis and extends to zero.

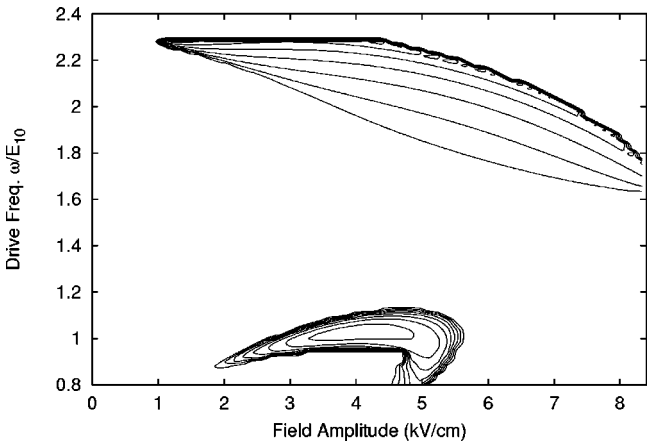

FIG. 11. Level sets displaying the regions of subharmonic generation in the two-subband asymmetric QW. Inner level sets represent a stronger subharmonic response. The level sets in the figure give the difference between maximum and minimum dipole moments obtained at each value of field amplitude and frequency from Poincaré maps. The sheet density is $N_s = 1.5 \times 10^{11}$ cm^{-2}.

B. Period doubling and Hopf bifurcations

The bifurcation diagram in Fig. 7 describes the collective electron oscillations. It shows the Poincaré map (strobe pictures taken at the drive frequency) of the dipole moment time flow $\langle \mu(t) \rangle = \mathrm{tr}\{\mu\, \sigma(t)\}$ plotted as a function of the field amplitude. A PDB in the Poincaré map occurs at 5.1 kV cm^{-1} followed by the appearence of a subcritical HB of the period-2 orbit (as the field increases) around 5.7 kV cm^{-1}. Around 6.6 kV cm^{-1} the torus (corresponding to the HB response) disappears abruptly and from it emerges a period-2 orbit which subsequently also disappears abruptly around 8.1 kV cm^{-1}. Further on our most interesting nonlinear bifurcation is observed around 11.3 kV cm^{-1}; this time when the field is decreased pass this value a direct HB of the period-1 orbit occurs, giving rise to a torus.

We found that when $N_s \approx 3.0 \times 10^{11}$ cm^{-2} the bifurcations occur with greatest strength and at the same time require a small field amplitude, while for $N_s < 0.5 \times 10^{11}$ cm^{-2} and for $N_s > 6.0 \times 10^{11}$ cm^{-2} the bifurcations become too small for practical observations. We also verified that the results of Fig. 7 persist qualitatively for different driving frequencies as can be seen in Fig. 8. It shows a contour plot of Poincaré-map sweeps. The level sets are obtained from the difference between maximum and minimum values of the dipole moment obtained at each field amplitude and frequency from the Poincaré map.

The phase portrait (a two-dimensional cross section) of the Poincaré map is shown in Fig. 9. It depicts the dipole moment plotted against its time derivative (on the vertical axis) for various values of field strength before and after the HB. Near 11.3 kV cm^{-1} a supercritical HB is observed as we decrease the field intensity; the fixed point, corresponding to a periodic orbit with the frequency of the drive, becomes unstable, generating a quasiperiodic orbit which is depicted as a small closed orbit in the phase portrait. Several of those orbits are plotted, each one corresponding to a fixed value of the field strength; decreasing the field amplitude gives rise to a new and larger closed orbit. The evidence of the quasiperiodic response can be seen from the filling of the closed orbits in Fig. 9.

The power spectrum before and after the HB is shown in Fig. 10. The large and broad peak close to $\omega/2$ is the main feature of the bifurcation. The peak in Fig. 10 is broad due to the difference frequencies, dressed $\pm(E_{21} - E_{10})$, which are clearly visible on each side of the incommensurate peak. The half-frequency peaks (not shown) for the PDB are sharp in distinction.[8] By varying the sheet density and field strength the incommensurate peak can be tuned but this will be explored in another study. In Fig. 10 there is also a dc response but it coincides with the zero-frequency axis and cannot be seen. The dynamics of the electron gas after (decreasing field amplitude) the HB corresponds to a quasiperiodic orbit on a torus defined by the incommensurate frequency and fundamental. At both the PDB and HB's the populations of the upper subbands are suddenly increased at the expense of the zeroth subband.

V. CONCLUSION

We obtained the equations of motion for electrons confined in δ-doped QW's in a systematic way, starting with the total Hamiltonian and culminating with the multisubband density-matrix equations in the time-dependent Hartree approximation. In this process we dealt carefully with the origin of the depolarization shift terms and included the contribution of the asymmetric terms of the Coulomb interaction coefficients in the Hamiltonian. We then adopted two different approaches to analyze the information provided by the equations of motion.

In the first approach we used a relatively new mathematical technique—the averaging method—as an alternative and more refined approach to the usual perturbation methods to simplify the equations of motion. With this method we studied the absorption line shapes and reobtained the usual depolarization shift due to the charge dynamical screening. Also, broadening and distortion (in QW's with $N_s > 10^{11}$ cm^{-2}) of the resonance peak due to high-intensity fields were observed in a two-subband system in qualitative agreement with experiments by Craig *et al.*[11] We found the necessary conditions for the observation of optical bistability using Eq. (31). Based on it we obtained Fig. 4, which can serve as a guide for the experimentalist in the search for an OB in QW's. From Fig. 4 one can see that the existence of positive detuning favors an OB response. Although OB, line broadening, and distorting of the absorption peak have already been predicted by other models,[13,30] we believe that our theoretical approach provides a more systematic way to study these phenomena. Also, our approach allows one to handle more complex situations such as the optical properties of many-subband QW's; we used this method to study the absorption lines of a three-subband system.

In the second approach we simply integrated the equations of motion obtained from Sec. II. For a two-subband QW we obtained an OB response in the absorption line in good agreement with the results obtained from the averaged equations. We also obtained the parameter range for subhar-

monic generation in an asymmetric double QW (shown in Fig. 11) (the outer contours in this figure correspond to PDB's). We did not analyze these PDB's here with the averaging method since some of us[17] were able to predict PDB's with the averaging method when the drive frequency is near twice the resonance frequency, but we had to go to second order in the averaging. For arbitrary drive frequencies this approach (second-order averaging) does not seem to be applicable to predict PDB's.

As the THz region of the spectrum is opened—for science and technology—the need arises for materials and structures exhibiting nonlinearities at the FIR frequencies. The detection of this type of response in *n*-doped QW's would indicate that the nonlinear density-matrix equations based on the time-dependent Hartree approximation are a good approximation for the infinite-dimensional many-body problem. This would strongly suggest that its other predictions such as PDB's and HB's will also be present if one searches in the appropriate parameter range. The realization that QW's can undergo a Hopf bifurcation (from a periodic orbit) only observed before in classical nonlinear systems may lead to applications such as frequency downconverters for electronic detection of amplitude-modulated FIR signals and new sources of FIR radiation.

ACKNOWLEDGMENTS

The authors would like to thank S. J. Allen and A. Imamoglu for helpful discussions. We thank the support by Grant Nos. NSF-DMR-0223770 and DARPA-Navy N00014-99-10935 (A.A.B. and B.B.), Proyectos UBACyT 2001-2 and Fundación Antorchas (PIT), NSF-ECS-0072986, the Office of Naval Research, and the Yamacraw program of the State of Georgia (A.A.B. and D.S.C.).

[1] C. Holmes and P. Holmes, J. Sound Vib. **78**, 161 (1981).
[2] J. Guckenheimer and P. Holmes, *Nonlinear Oscillations, Dynamical Systems, and Bifurcations of Vector Fields* (Springer-Verlag, New York, 1983).
[3] F. Dalfovo, S. Giorgini, L.P. Pitaevskii, and S. Stringari, Rev. Mod. Phys. **71**, 463 (1999).
[4] P.W. Anderson, *Lectures on the Many-Body Problem* (Academic Press, New York, 1964).
[5] P. Grangier *et al.*, Phys. Rev. A **46**, 2735 (1992).
[6] H. Haug and S.W. Koch, *Quantum Theory of the Optical and Electronic Properties of Semiconductors* (World Scientific, Singapore, 1990).
[7] J.N. Heyman *et al.*, Phys. Rev. Lett. **72**, 2183 (1994).
[8] B. Galdrikian and B. Birnir, Phys. Rev. Lett. **76**, 3308 (1996).
[9] J.N. Heyman *et al.*, Phys. Rev. Lett. **74**, 2682 (1995).
[10] M.S. Sherwin *et al.*, Physica D **83**, 229 (1995).
[11] K. Craig *et al.*, Phys. Rev. Lett. **76**, 2382 (1996).
[12] M. Zaluẓny, Phys. Rev. B **47**, 3995 (1993).
[13] M. Zaluẓny, J. Appl. Phys. **74**, 4716 (1993).
[14] T. Ando, Z. Phys. B **24**, 33 (1976).
[15] S.J. Allen, Jr., D.C. Tsui, and B. Vinter, Solid State Commun. **20**, 425 (1976).
[16] The Hopf bifurcation is well known to be related to the Ruelle-Takens quasiperiodic route to chaos in classical systems (Ref. 35).
[17] A.A. Batista, B. Birnir, and M.S. Sherwin, Phys. Rev. B **61**, 15 108 (2000).
[18] S.L. Chuang, M.S.C. Luo, S. Schmitt-Rink, and A. Pinczuk, Phys. Rev. B **46**, 1897 (1992).
[19] M.S.C. Luo, S.L. Chuang, S. Schmitt-Rink, and A. Pinczuk, Phys. Rev. B **48**, 11 086 (1993).
[20] D.E. Nikonov, A. Imamoglu, L.V. Butov, and H. Schmidt, Phys. Rev. Lett. **79**, 4633 (1997).
[21] D.E. Nikonov, A. Imamoglu, and M.O. Scully, Phys. Rev. B **59**, 12 212 (1999).
[22] L. Tsang, C. Chansungsan, and S.L. Chuang, Phys. Rev. B **45**, 11 918 (1992).
[23] A.L. Fetter and J. Walecka, *Quantum Theory of Many-Particle Systems* (McGraw-Hill, San Francisco, 1971).
[24] R. Decca *et al.*, Phys. Rev. Lett. **72**, 1506 (1994).
[25] P.I. Tamborenea and S. Das Sarma, Phys. Rev. B **49**, 16 821 (1994).
[26] F. Verhulst, *Nonlinear Differential Equations and Dynamical Systems* (Springer-Verlag, New York, 1996).
[27] J. A. Sanders and F. Verhulst, *Averaging Methods in Nonlinear Dynamical Systems* (Springer-Verlag, New York, 1985).
[28] N. Peyghambarian, S.W. Koch, and A. Mysyriwicz, *Introduction to Semiconductor Optics* (Prentice-Hall, Englewood Cliffs, NJ, 1993).
[29] M. Seto and M. Helm, Appl. Phys. Lett. **60**, 859 (1992).
[30] M.I. Stockman *et al.*, Phys. Rev. B **48**, 10 966 (1993).
[31] J.B. Williams, K. Craig, M.S. Sherwin, K. Campman, and A.C. Gossard, Physica E **2**, 177 (1998).
[32] J.B. Williams, M.S. Sherwin, K.D. Maranowski, and A.C. Gossard, Phys. Rev. Lett. **87**, 037401 (2001).
[33] C.A. Ullrich and G. Vignale, Phys. Rev. Lett. **87**, 037402 (2001).
[34] These linewidths are primarily determined by Γ_2 at low field intensities. So far no experiments were made to determine Γ_2 for high field intensities. Also to our knowledge no experiments have been made to determine relaxation rates in three- or more-subband QW's.
[35] J.D. Crawford, Rev. Mod. Phys. **63**, 991 (1991).